Journal of Zhejiang University-SCIENCE A (Applied Physics & Engineering)
ISSN 1673-565X (Print); ISSN 1862-1775 (Online)
www.jzus.zju.edu.cn; www.springerlink.com
E-mail: jzus@zju.edu.cn

Filtration of micro-particles within multi-fiber arrays by adhesive DEM-CFD simulation*

Ran TAO, Meng-meng YANG, Shui-qing LI†‡

Key Laboratory for Thermal Science and Power Engineering of Ministry of Education, Department of Thermal Engineering, Tsinghua University, Beijing 100084, China

†E-mail: lishuiqing@mail.tsinghua.edu.cn

Received Mar. 24, 2017; Revision accepted Oct. 29, 2017; Crosschecked Dec. 15, 2017

Abstract: A 3D multi-time scale discrete element method-computational fluid dynamic (DEM-CFD) coupling approach was applied to investigate the filtration of micron-sized particles by different types of fiber arrays. Both the pressure drop and the filtration efficiency were examined to indicate the filtration performance of the fiber arrays. Fibers that were uniformly arrayed in a parallel or staggered manner were compared. Results showed that the staggered array showed a better performance than the parallel array in terms of both pressure drop and filtration efficiency. Further, we compared the performance of different staggered arrays, i.e. a regular case, one densified in the front layers and another densified in the back layers. The front densified array was found to enter the clogging and cake filtration stage in the shortest time, leading to the highest filtration efficiency, but the highest pressure drop. The back densified array still achieved a much higher filtration efficiency, despite a much lower pressure drop comparable to that of the regular array. The results suggest that the two kinds of densified arrays may be suited for different purposes, e.g. baghouse filters or breathing masks.

Key words: Filtration; Fiber arrays; Staggered arrays; Discrete element method (DEM)
https://doi.org/10.1631/jzus.A1700156 **CLC number:** TK09

1 Introduction

Fiber filtration is a both highly-efficient and cost-effective way to remove particles from gaseous fluid. Due to its great versatility and adaptability, fiber filtration has been widely used in various industrial fields, such as in power plants, air purification, and cement industries (Li and Marshall, 2007; Kasper et al., 2010; Dunnett and Clement, 2012; Kolakaluri et al., 2015; LaMarche et al., 2016). In recent years, with the urgency to improve air quality in China, more attention has been paid to the control of airborne pollutants, especially for micron-sized particles such as $PM_{2.5}$.

Various studies have been devoted to the process of fiber filtration by both experiments and computer simulations (Kanaoka et al., 1980; Myojo et al., 1984; Dittler et al., 1998; Thomas et al., 1999; Karadimos and Ocone, 2003; Dunnett and Clement, 2006; Roussel et al., 2007; Schiller and Schmid, 2015). Some crucial macroscopic operational parameters, such as the pressure drop and filtration efficiency, have been obtained by experiments. Three different stages, the clean filter stage, the clogging stage, and the cake filtration stage (Thomas et al., 1999), have been identified on the basis of the pressure drop variation, and have enhanced understanding of the whole process. A series of models as well as some empirical expressions have also been presented to describe the pressure drop and the filtration efficiency under various operational conditions (Myojo et al., 1984;

‡ Corresponding author
* Project supported by the National Key Research and Development Program of China (No. 2017YFB0603203) and the National Natural Science Foundation of China (No. 51390491)
ORCID: Ran TAO, https://orcid.org/0000-0003-0073-7339

Novick et al., 1990; Thomas et al., 2001; Tien et al., 2001; Kasper et al., 2009). However, these expressions usually apply only under specific limited conditions, and most are validated only for single fiber filtration systems, which could be quite different from realistic filtration systems in both industries and labs. Moreover, few of these studies have considered the effect of deposited particles on the air flow field during the particle deposition process, leading to an overestimation of the filtration efficiency.

Some studies have attempted to correlate the filtration efficiency of a fiber array system consisting of several layers with that of a single fiber system (Flagan and Seinfel, 1988; Liu and Wang, 1997). However, these correlations did not consider the different geometrical arrangements of fiber arrays. Different geometrical arrangements will surely affect the filtration performance, which calls for in-depth studies to divulge the underlying mechanisms of particle capture during the filtration process. This study is of great significance to industry because real filters used in precipitators are fabricated in different arrangements. It was also our motivation to relate the outcomes of this study to the performance of practical particle-loaded filters.

Due to the limitations of existing measuring tools, experimental results have not yet provided the microscopic information needed to understand the underlying physics of filtration mechanisms. As a consequence, computer simulation is becoming more widely recognized as a promising approach. Dozens of studies have been published using different numerical approaches, and both 2D and 3D fiber filtration processes have been simulated (Karadimos and Ocone, 2003; Maze et al., 2007; Wang and Pui, 2009; Hosseini and Tafreshi, 2010; Dunnett and Clement, 2012; Wang et al., 2013). However, for the filtration problem considered here, the two-way coupling between the particle and fluid phases has been shown to have a significant impact on the filtration efficiency (Karadimos and Ocone, 2003; Li et al., 2011).

Based on the studies using the discrete element method (DEM) (Tomas, 2007; Luding, 2008; Liu et al., 2016; Tamadondar et al., 2017), recently we developed a new approach combining DEM with computational fluid dynamics (CFD) (the DEM-CFD approach), which has both a relatively low computational cost and a high calculation accuracy. Our DEM method, based on the Johnson, Kendall, Roberts (JKR) contact mechanics model, has been shown to have high precision in obtaining the dynamic behavior of micro-particles, in which van der Waals adhesive force plays a significant role in determining particle motion (Li and Marshall, 2007; Li et al., 2011; Yang et al., 2013; Liu et al., 2015; Chen et al., 2016a). The combining of DEM and CFD realizes the two-way coupling between solid particles and the fluid phase, which has been applied to the clogging process with consistent results (Chen et al., 2016a). This two-way coupling method is a promising approach for elucidating the geometrical effect of fiber arrays on filtration performance.

This paper presents the filtration performance of fiber arrays with different types of geometrical arrangements. First, we provide a brief introduction to our adhesive DEM-CFD coupling approach. Then, we compare the simulation results of a parallel array and a staggered array to discuss the effect of fiber arrays. Thirdly, we further discuss different kinds of geometrical arrangements of staggered arrays, either front densified or back densified, and compare their performance. Finally, conclusions are drawn from the comparisons among the different fiber arrays.

2 Computational methods

In this work, the adhesive DEM-CFD coupling method was developed and employed. The particle phase was numerically simulated by the adhesive DEM based on JKR contact theory (Li and Marshall, 2007; Li et al., 2011; Chen et al., 2016b), while the gas phase governing equations for mass and momentum conservation were solved by open-source MFIX code (Garg et al., 2012; Li et al., 2012). In particular, the two-way coupling between the phases was built on a multi-time-step approach.

2.1 Equations for gas phase

The governing equations of the gas phase were solved under the assumption of an incompressible fluid with constant dynamic viscosity and fluid density, and are written as

$$\begin{aligned} &\frac{\partial \varepsilon_{\mathrm{g}}}{\partial t}+\nabla\cdot\left(\varepsilon_{\mathrm{g}}\boldsymbol{u}\right)=0,\\ &\frac{\mathrm{D}}{\mathrm{D}t}\left(\varepsilon_{\mathrm{g}}\rho_{\mathrm{g}}\boldsymbol{u}\right)=\nabla\cdot\boldsymbol{S}_{\mathrm{g}}-\boldsymbol{I}_{\mathrm{gs}}, \end{aligned} \tag{1}$$

where ε_g is the gas phase volume fraction, ρ_g is the density of the gas, $\boldsymbol{u}$ is the volume-averaged gas velocity, and $\boldsymbol{S}_g$ is the stress tensor of the gas. $\boldsymbol{I}_{gs}$ is the momentum transfer term between the gas and solid phases. This term represents the disturbance of particle motion in the gas and is determined according to the drag from the solid particles. The two-way coupling between the solid and gas phases is essential for problems such as particle deposition on fibers and micron-particle packing under the fluid effect (Zhu et al., 2008).

2.2 Adhesive DEM for particle phase

The linear and angular momentum equations were solved by our adhesive DEM as follows:

$$\begin{aligned} m\frac{\mathrm{d}\boldsymbol{v}}{\mathrm{d}t} &= \boldsymbol{F}_g + \boldsymbol{F}_{ad}, \\ I\frac{\mathrm{d}\boldsymbol{\Omega}}{\mathrm{d}t} &= \boldsymbol{M}_g + \boldsymbol{M}_{ad}, \end{aligned} \tag{2}$$

where m is the particle mass, I is the moment of inertia, $\boldsymbol{v}$ is the translational velocity, and $\boldsymbol{\Omega}$ is the rotation rate of a single particle. $\boldsymbol{F}_g$ is the hydrodynamic force and $\boldsymbol{M}_g$ the torque exerted on an individual particle. $\boldsymbol{F}_{ad}$ is the adhesive contact force and $\boldsymbol{M}_{ad}$ the adhesive torque in collisions with other particles.

Particles in a viscous fluid such as air are subjected to many different kinds of hydrodynamic forces and torques. However, the dominant ones in our filtration problem, which in essence is particles moving in a flow at small Reynolds number Re, are the viscous drag force and torques, which can be given respectively as

$$\begin{aligned} \boldsymbol{F}_{drag} &= -3\pi\mu d_p(\boldsymbol{v}-\boldsymbol{u})f, \\ \boldsymbol{M}_{drag} &= -\pi\mu d_p^3(\boldsymbol{\Omega}-\frac{1}{2}\omega_g), \end{aligned} \tag{3}$$

where μ is the gas dynamic viscosity, d_p is the particle diameter, and ω_g is the gas vorticity. f is the friction factor, which is used to correct for particle crowding and particle inertia. f is obtained using the drag correlation applicable to the range of 0.01 to 1000 for Re (Benyahia et al., 2006). The friction factor was set at 0.3 in our cases.

The adhesive contact force in the normal direction, F_n, contains two terms, the elastic and adhesive force F_{ne} and the normal dissipative force F_{nd}. F_{ne} is based on the JKR model which takes account of both the elastic deformation and van der Waals adhesion of colliding particles (Johnson et al., 1971). F_{nd} is assumed to be proportional to the approaching velocity of colliding particles, $\boldsymbol{v}_R$. The forces and torques in other directions, including sliding, twisting, and rolling, have also been considered previously (Li and Marshall, 2007; Marshall, 2009). Details of these models can be found in the studies of Li et al. (2011) and Marshall and Li (2014).

3 Results and discussion

3.1 Comparison between parallel and staggered arrays

The computer simulation was performed in a 3D rectangular domain, in which fibers are arranged in different types of arrays. Here we used the fiber radius r_f as the characteristic length L in order to non-dimensionalize. The computational domain was set up in the ranges of $-15\le X^*\le+1$, $-4\le Y^*\le+4$, and $-2\le Z^*\le+2$, where X^*, Y^*, and Z^* are the non-dimensional positions with respect to L in a Cartesian coordinate. The gas flows along the direction X with particles captured by the fibers fixed in the domain. Periodic conditions were applied in both the Y and Z directions.

In this section, with the aim of comparing the filtration performance of parallel and staggered arrays, we positioned the fibers as shown in Fig. 1. In both arrays, three layers of fibers were positioned at $X^*=-4$, 0, +4. In each layer, the fiber separation, W, which is defined as the distance between the centers of two adjacent fibers, was kept constant at $4L$. For the parallel array, all fibers were positioned at $Y^*=\pm2$, while for the staggered array, the layer in the middle (positioned at $X^*=0$) was different from the other two layers, with fibers positioned at $Y^*=0, \pm4$. The fluid field in Fig. 1 was normalized by the superficial filtration velocity, U, which was also the initial gas and particle velocity at the inlet. Particles entered the simulation domain with random initial positions at the inlet and were assumed to be neutrally buoyant without the effect of gravity.

The main physical parameters used in our simulation are listed in Table 1. The superficial filtration velocity was 0.2 m/s. The fiber radius was 10 μm,

which was determined based on the real size of fibrous material normally used in industry. The particle radius was set at 1 μm, which can well represent micron particulate matter with an aerodynamic diameter smaller than 2.5 μm. Note that the values of particle mass density (2500 kg/m^3) and work of adhesion (20.0 mJ/m^2) were typical of micron-sized particles widely found in existing environments. With these parameters, the critical velocity for particle head-on collisions was obtained as about 0.618 m/s (Chen et al., 2015), which is actually larger than the superficial filtration velocity.

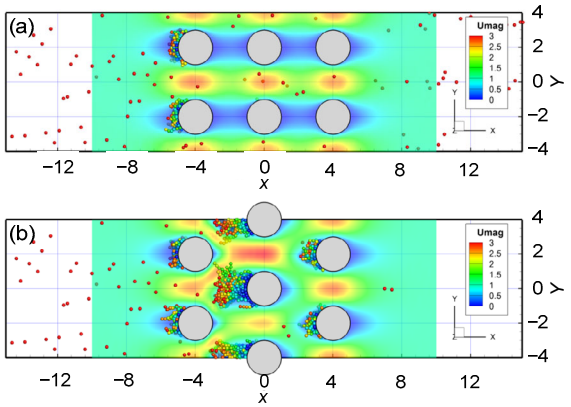

Fig. 1 Schematics of simulated domains with a parallel array (a) and a staggered array (b) viewed from above
Umag represents the fluid velocity non-dimensionalized by the superficial filtration velocity

Table 1 Physical parameters used in simulations

Physical parameter	Value
Particle and fiber	
Particle radius, r_p (μm)	1.0
Fiber radius, r_f (μm)	10.0
Particle mass density, ρ_p (kg/m^3)	2500
Elastic modulus, E (Pa)	2×10^7
Poisson's ratio, σ	0.33
Restitution coefficient, e	0.8
Work of adhesion, w (mJ/m^2)	20.0
Gas	
Gas viscosity, μ (Pa·s)	1.79×10^{-5}
Gas density, ρ_g (kg/m^3)	1.25
Superficial filtration velocity, U (m/s)	0.2

The variation of the simulated pressure drop was characterized both with dimensionless time and deposited particle numbers (Fig. 2). The time was non-dimensionalized by L/U, which was also equal to r_f/U in our cases. For the same number of captured particles, the staggered array always had a lower pressure drop than the parallel array (Fig. 2a). This is because in the staggered array, particles tended to deposit on the first two layers of fibers (there were actually five fibers), while in the parallel array, particles were deposited mainly on the first layer alone (there were only two fibers). As a result, clogging occurred between the two fibers in the first layer with fewer deposited particles in the parallel array.

Interestingly, the apparent pressure drop difference between these two arrays lay in a specific period when the deposited particle number was from 1000 to 4500, which approximately coincided with the clogging stage and the early stage of cake filtration. In practical filtration systems, most particles are captured during the cake filtration stage, and in this stage the pressure drop is the most important concern. At an identical number of captured particles, a much lower pressure drop is expected to lower the operational costs of power plants. Fig. 2b describes the variation of the pressure drop with the dimensionless time. The three stages, including the clean filter stage, the clogging stage, and the cake filtration stage, are separated by two segmentation points, with both the deposited particle number and the dimensionless time presented in Table 2. It is apparent that the staggered array entered into the clogging stage and the subsequent cake filtration stage much earlier than the parallel array. That is, the time it took for the parallel array to end the clean filter stage was more than twice that taken by the staggered array. As a result, the staggered array could efficiently shorten the initial clean filter stage of filtration, avoiding more penetrating particles.

Table 2 Deposited particle number N_{dep} and dimensionless time T^* at the end of two stages

Array type	Clean filter stage		Clogging stage	
	N_{dep}	T^*	N_{dep}	T^*
Parallel	1364	1595	2586	1915
Staggered	2560	737	4483	1216

Apart from the pressure drop, the filtration efficiency was examined (Fig. 3a). Even in the initial clean filter stage in which particles easily penetrate,

the filtration efficiency of the staggered array (around 0.76) was significantly higher than that of the parallel array (around 0.14) (Fig. 3a). The initial filtration efficiency of the parallel array was quite close to that of a two-fiber system. This is reasonable because the successive fibers behind the first layer of the parallel array rarely help capture particles, as envisioned in Fig. 1a.

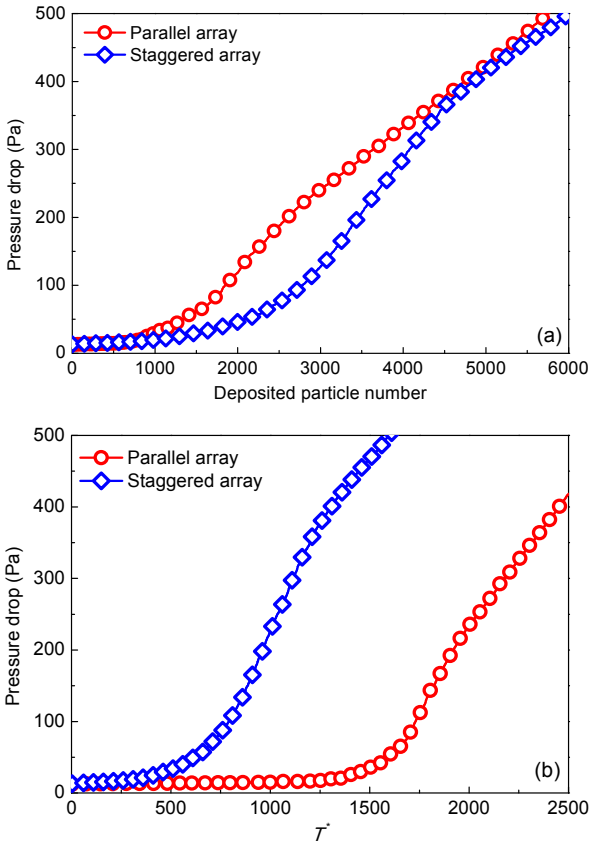

Fig. 2 Pressure drop variation with deposited particle number (a) and dimensionless time (b)

However, for the staggered array of fibers, particles that penetrate through the front layer will run into the subsequent layer and still have an opportunity to be captured. This dramatically increases the filtration efficiency in the initial clean filter stage and even the clogging stage. Note that the filtration efficiency decreased only slightly from about 0.81 to 0.76 in the clean filter stage. This is due mainly to the hydrodynamic effect of the deposited particles on the fluid field, which results in more particles flowing with the fluid and crossing the staggered fibers. It is more intuitive if we compare the penetrating particle numbers as depicted in Fig. 3b. Particles kept penetrating until the filtration efficiency reached unity, signaling a transition from the clogging stage to the cake filtration stage. The final number of penetrating particles is another indicator of overall filtration performance.

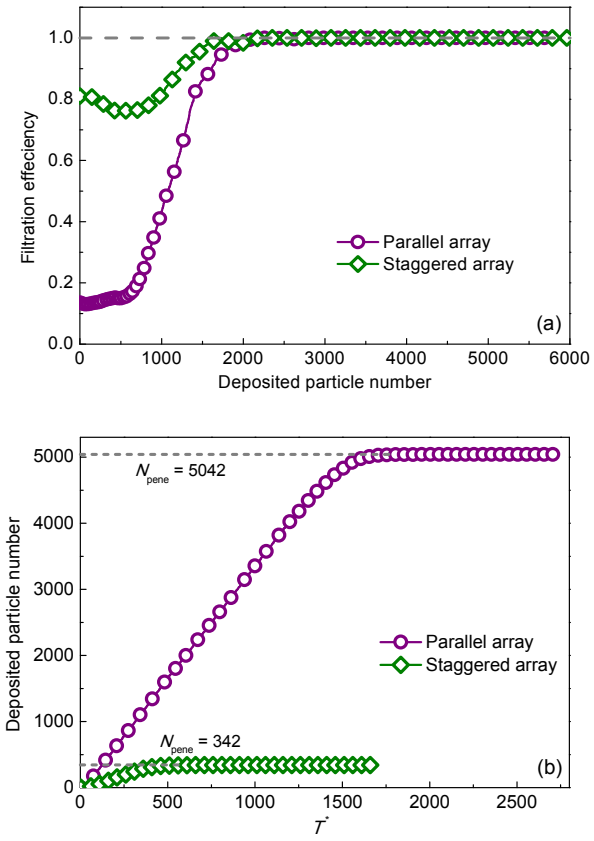

Fig. 3 Filtration efficiency as a function of deposited particle number (a) and penetrating particle number N_{pene} as a function of dimensionless time (b)

The penetrating particle number for the parallel array (around 5042) was nearly fifteen times that for the staggered array (342). This implies that fewer particles will penetrate when the filtration process enters the clogging and cake filtration stages earlier, as already discussed for Fig. 2b.

Different from the 'frozen' assumption widely used in the literature (Karadimos and Ocone, 2003; Hosseini and Tafreshi, 2010), the real dynamic simulation achieved by adhesive DEM is of importance for building the micro-structures of deposited particles during progressive filtration. For instance, we found that during the initial part of the clean filter

stage, particles loading on the fibers formed chains due to adhesion between two contacting particles. However, as the filtration proceeded, the particle chains lodged down onto the fibers and enlarged the capture area, as can be seen clearly from Fig. 4. The lodged particle chains had a great impact on the pressure drop and the filtration efficiency (Li et al., 2011) as well as the deposition structure of particles, which is also a crucial aspect for determining the mechanisms of fiber filtration.

3.2 Comparison between different densification modes of the staggered array

A staggered array performs well from the viewpoints of both the pressure drop and filtration efficiency. Therefore, we further compared the filtration performance of the staggered array with two different modes of densification, which we believed would be helpful for the advanced design of practical filters.

Fig. 5 schematically shows the fiber arrays under different densification modes. Fig. 5a shows a regularly staggered array. It includes five layers of fibers positioned with a layer distance of $4L$. In each layer, the fiber separation, W, was kept as $6L$. We then arbitrarily densified the arrangement of fibers in a layer by changing the fiber separation from $6L$ to $4L$, and we set up the cases of two densification modes. In one case the densification was in the two front layers (Fig. 5b), and in the other case it was in the two back layers (Fig. 5c). The other model parameters were all the same as those given in Table 1. Note that compared to the computational domain in the previous section, the domain was enlarged in the Y-direction, spanning from Y^*=−6 to Y^*=+6.

Firstly, the pressure drop was compared for the three cases. Fig. 6 presents the pressure drop variation with the deposited particle number and the dimensionless time. The staggered array with densification in the two front layers had a notably higher pressure drop when the number of particles captured was the same (Fig. 6a). Fig. 5 shows the side views with 3000 particles captured for all three cases. As shown in Fig. 5b, more particles were deposited on the two front layers of fibers, in contrast to both the regular and back densified cases. Consequently, there was

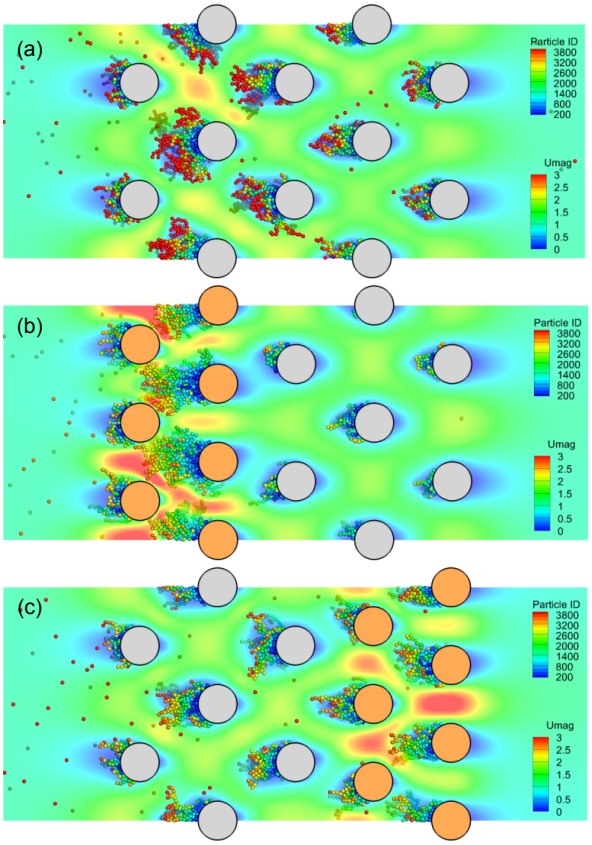

Fig. 5 Schematics of the regular staggered array (a), the staggered array densified in the two front layers (b), and the staggered array densified in the two back layers (c)

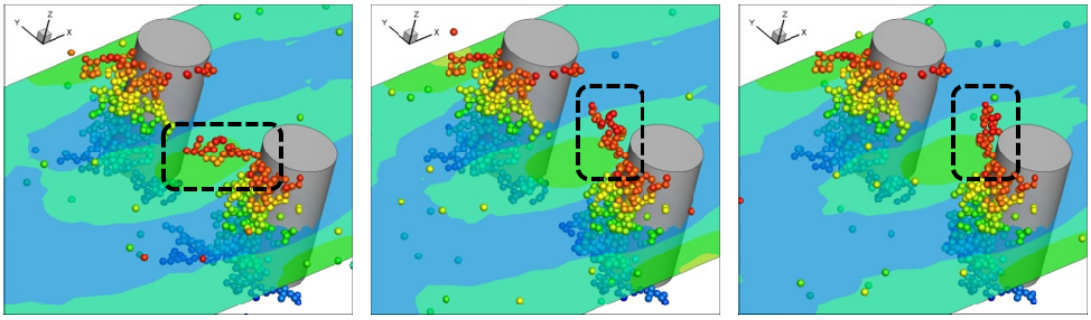

Fig. 4 Lodging of particle chains on the first fiber layer (marked by the dashed box) from T^*=1675 to T^*=1685 for the parallel array

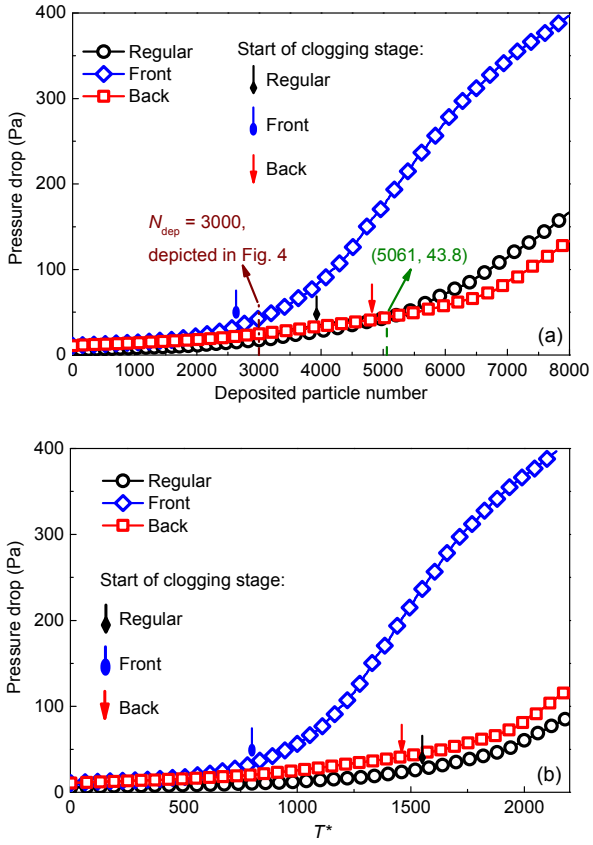

Fig. 6 Pressure drop variation with deposited particle number (a) and dimensionless time (b). "Regular" represents the case with regular staggered array, and "front" and "back" represent cases with densification in front layers and back layers, respectively

much less space for fluid to pass through these layers, and the fluid was driven to flow with higher velocity (red color in Fig. 5), which finally caused a much higher pressure drop than that in the regular case.

To our surprise, the back densified case showed a remarkably lower pressure drop than the front densified case when 3000 particles were captured. This is because, even in the back densified case, there were still a considerable number of particles deposited in the first three loose layers, which apparently reduced the number of particles in the densified layers as well as the fluid velocity and pressure drop. In other words, the particles were distributed more evenly in the back densified case than those in the front densified case, which had particles deposited mostly in the two front layers, thus causing a larger pressure drop. Furthermore, the values of pressure drop for the back densified case and the regular case were very similar, as detailed in Fig. 6. When the deposited particle number reached 5061, the pressure drop in the regular case exceeded that in the back densified case (Fig. 6a). This is because the regular case can enter the clogging stage with much fewer deposited particles, causing the faster increase in the pressure drop.

It is apparent that the front densified case took the shortest time to enter the clogging stage and then the cake filtration stage (Fig. 6b). In both the regular staggered case and the back densified case, it took longer to enter the clogging stage. The back densified case entered the clogging stage a little earlier than the regular staggered case.

The filtration efficiency for the three cases is shown in Fig. 7a. According to the curves of all three cases, we found that the filtration efficiency first oscillated for some time, and then kept increasing until reaching unity. Thus, we analyzed the oscillating period and obtained the number of particles at which the curve stopped oscillating and started moving up continuously. These numbers are denoted as N_o, N_f, and N_b in Fig. 7a. The values indicate that the regular staggered array needed the most particles to go through the oscillating time, and that the front densified array needed the fewest. After the oscillating period, the filtration efficiency for the front densified case increased to unity with the fewest particles captured. The filtration efficiency for the other two cases reached unity at a similar number of particles.

The numbers of penetrating particles for the three cases are shown in Fig. 7b, which gives a fairly favorable characterization of the overall performance. With only 538 particles penetrating through at the end, the front densified array clearly showed the best performance. Note that this number cannot be directly compared with the penetration particle number of 342 for the staggered case in the previous section, because in this simulation the computational domain was larger (with Y^* spanning from −6 to +6). For the regular array and the back densified array, although their filtration efficiency reached unity at a similar number of deposited particles, the penetrating particle numbers were quite different. With the value of 2281, the penetrating particle number for the regular case was more than twice that for the back densified case. This is due to the difference in the particle capture efficiency before it finally reached unity. As a result, the

back densified array had a better overall filtration performance than the regular array.

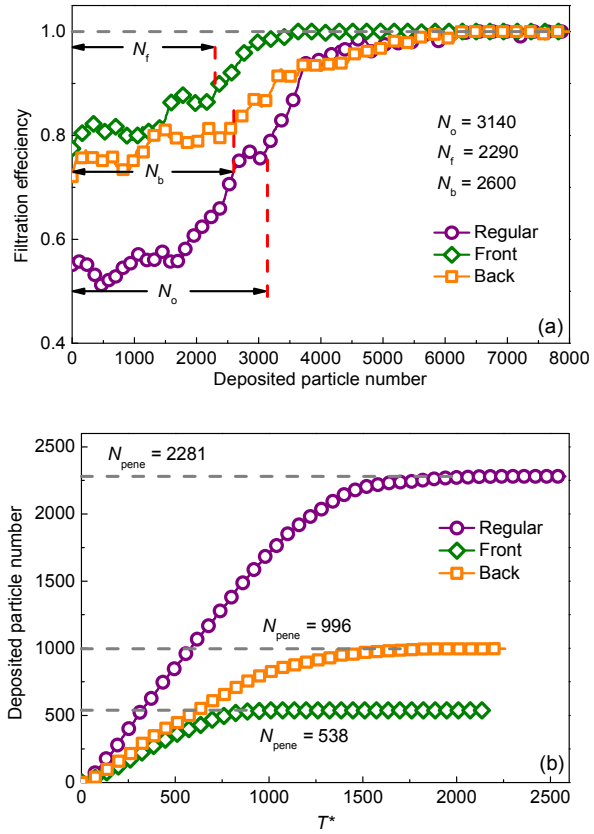

Fig. 7 Filtration efficiency as a function of deposited particle number (a) and penetrating particle number as a function of dimensionless time (b). N_o, N_f, and N_b are the numbers of particles for the oscillating period relating to the regular, front densified, and back densified arrays, respectively

Finally, we analyzed the probability distribution of deposited particles before they began clogging. Again, we took the number of deposited particles as 3000, the same as in the side views in Fig. 5. The probability distribution functions for the three cases along the *X*-direction are shown in Fig. 8. First, for the regular staggered array, the second layer captured most particles and had the highest peak. The other four layers captured a similar number of particles. This suggests that the second layer rather than the first plays the most crucial role in capturing particles. Clearly, the computer simulation of multi-layer filters is important in elucidating the underlying physics of the filtration process, which cannot be revealed by the simulation of one-layer, two-fiber systems, let alone the widespread single-fiber systems.

Compared to the regular case, the front densified array reinforced the effect of the first two layers and thus had fewer particles captured by the three layers at the back. This is much more convenient for the frequent cleaning of dust from filters (e.g. a baghouse filter) and their long-term use, because most particles stay in the front layers and do not penetrate deeply. For the back densified case, more particles were captured by the two layers at the back. The particles penetrating the first several layers had a good chance of being captured by the last two layers, which accounts for its higher filtration efficiency than the regularly staggered array. Considering the much lower pressure drop in comparison with the front densified case, this suggests that the back densified array should be used for disposable filtration devices, e.g. personal breathing masks. Users may benefit from the comfort of a lower pressure drop while breathing the air, and the device is used only once without dust cleaning.

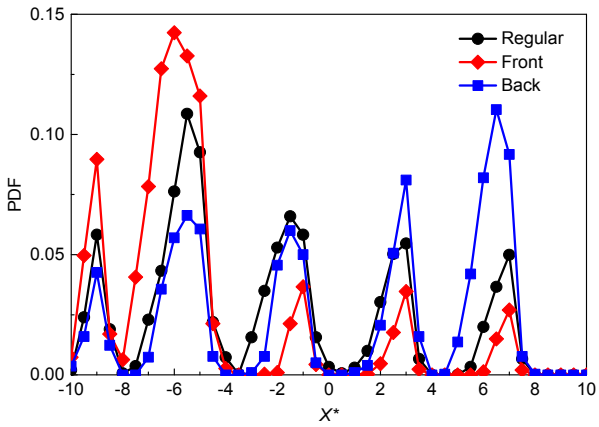

Fig. 8 Probability distribution function (PDF) of particles deposited along the *X*-direction (when the deposited particle number equaled 3000)

4 Conclusions

The 3D computer simulations of fiber filtration of micro-particles were performed using a newly developed adhesive DEM-CFD method, in which

two-way coupling between the gas and particle phases is realized by a multi-time-step approach. The models of inter-particle adhesion, dissipation, and frictions are based on the JKR theory. In this study, the geometrical effects of different kinds of fiber arrays on the mesoscopic physics of the filtration process were examined in detail.

Firstly, we compared the parallel and staggered arrays of fibers. The staggered array entered the clogging stage in a much shorter time, about 46% of that for the parallel array, and had a relatively low pressure drop at the same number of captured particles. The filtration efficiency of the staggered array in the initial clean filter stage was significantly higher than that of the parallel array. The penetrating particle number of the staggered array was about one-fifteenth of that of the parallel array, suggesting a better overall filtration.

Secondly, we compared the performance of different types of densification in the staggered array. The front densified array entered the clogging stage within a significantly shorter time (about 52% of that for the regular array and 55% of that for the back densified array). It also demonstrated a higher pressure drop with the same number of particles captured. The back densified array and the regular array showed a similar pressure drop during the filtration process. However, the back densified array had a better filtration efficiency than the regular array, although the front densified array performed best with the fewest particles passing through.

Finally, the probability distribution function of the deposited particle positions showed that the deposit structure of different arrays varied markedly. For the front densified array, about 83% of all deposited particles were located in the first two layers, compared with only 48% for the regular array. For the back densified array, about 52% of all deposited particles were captured by the last two layers, compared with only 10% for the regular array. These results will help enhance understanding of the underlying physics of fiber filtration with different geometrical arrangements.

Acknowledgments

The authors are grateful to Prof. Jeffrey S. MARSHALL (University of Vermont, USA), and grateful to Dr. Guan-qing LIU, Dr. Huang ZHANG, Mr. Wen-wei LIU, and Mr. Sheng CHEN (Tsinghua University, China) for their useful discussions.

References

Benyahia S, Syamlal M, O'Brien TJ, 2006. Extension of Hill–Koch–Ladd drag correlation over all ranges of Reynolds number and solids volume fraction. *Powder Technology*, 162(2):166-174. https://doi.org/10.1016/j.powtec.2005.12.014

Chen S, Li S, Yang M, 2015. Sticking/Rebound criterion for collisions of small adhesive particles: effects of impact parameter and particle size. *Powder Technology*, 274: 431-440. https://doi.org/10.1016/j.powtec.2015.01.051

Chen S, Liu W, Li S, 2016a. Effect of long-range electrostatic repulsion on pore clogging during microfiltration. *Physical Review E*, 94(6):063108. https://doi.org/10.1103/PhysRevE.94.063108

Chen S, Li S, Liu W, et al., 2016b. Effect of long-range repulsive coulomb interactions on packing structure of adhesive particles. *Soft Matter*, 12(6):1836-1846. https://doi.org/10.1039/C5SM02403J

Dittler A, Gutmann B, Lichtenberger R, et al., 1998. Optical in situ measurement of dust cake thickness distributions on rigid filter media for gas cleaning. *Powder Technology*, 99(2):177-184. https://doi.org/10.1016/S0032-5910(98)00102-8

Dunnett SJ, Clement CF, 2006. A numerical study of the effects of loading from diffusive deposition on the efficiency of fibrous filters. *Journal of Aerosol Science*, 37(9):1116-1139. https://doi.org/10.1016/j.jaerosci.2005.08.001

Dunnett SJ, Clement CF, 2012. Numerical investigation into the loading behaviour of filters operating in the diffusional and interception deposition regimes. *Journal of Aerosol Science*, 53:85-99. https://doi.org/10.1016/j.jaerosci.2012.06.008

Flagan CR, Seinfel HJ, 1988. Fundamentals of Air Pollution Engineering. Prentice Hall, Englewood Cliffs, New Jersey, USA, p.433-455.

Garg R, Galvin J, Li T, et al., 2012. Open-source MFIX-DEM software for gas–solids flows: part I—verification studies. *Powder Technology*, 220:122-137. https://doi.org/10.1016/j.powtec.2011.09.019

Hosseini SA, Tafreshi HV, 2010. 3-D simulation of particle filtration in electrospun nanofibrous filters. *Powder Technology*, 201(2):153-160. https://doi.org/10.1016/j.powtec.2010.03.020

Johnson KL, Kendall K, Roberts AD, 1971. Surface energy and the contact of elastic solids. *Proceedings of Royal Society London A: Mathematical, Physical and Engineering Sciences*, 324(1558):301-313. https://doi.org/10.1098/rspa.1971.0141

Kanaoka C, Emi H, Myojo T, 1980. Simulation of the growing process of a particle dendrite and evaluation of a single fiber collection efficiency with dust load. *Journal of Aerosol Science*, 11(4):383-385. https://doi.org/10.1016/0021-8502(80)90046-4

Karadimos A, Ocone R, 2003. The effect of the flow field recalculation on fibrous filter loading: a numerical simulation. *Powder Technology*, 137(3):109-119. https://doi.org/10.1016/S0032-5910(03)00132-3

Kasper G, Schollmeier S, Meyer J, et al., 2009. The collection efficiency of a particle-loaded single filter fiber. *Journal of Aerosol Science*, 40(12):993-1009. https://doi.org/10.1016/j.jaerosci.2009.09.005

Kasper G, Schollmeier S, Meyer J, 2010. Structure and density of deposits formed on filter fibers by inertial particle deposition and bounce. *Journal of Aerosol Science*, 41(12):1167-1182. https://doi.org/10.1016/j.jaerosci.2010.08.006

Kolakaluri R, Murphy E, Subramaniam S, et al., 2015. Filtration model for polydisperse aerosols in gas-solid flow using granule-resolved direct numerical simulation. *AIChE Journal*, 61(11):3594-3606. https://doi.org/10.1002/aic.14901

LaMarche CQ, Miller AW, Liu P, et al., 2016. Linking micro-scale predictions of capillary forces to macro-scale fluidization experiments in humid environments. *AIChE Journal*, 62(10):3585-3597. https://doi.org/10.1002/aic.15281

Li SQ, Marshall JS, 2007. Discrete element simulation of micro-particle deposition on a cylindrical fiber in an array. *Journal of Aerosol Science*, 38(10):1031-1046. https://doi.org/10.1016/j.jaerosci.2007.08.004

Li SQ, Marshall JS, Liu GQ, et al., 2011. Adhesive particulate flow: the discrete-element method and its application in energy and environmental engineering. *Progress in Energy and Combustion Science*, 37(6):633-668. https://doi.org/10.1016/j.pecs.2011.02.001

Li T, Garg R, Galvin J, et al., 2012. Open-source MFIX-DEM software for gas-solids flows: part II—validation studies. *Powder Technology*, 220:138-150. https://doi.org/10.1016/j.powtec.2011.09.020

Liu D, van Wachem BGM, Mudde RF, et al., 2016. An adhesive CFD-DEM model for simulating nanoparticle agglomerate fluidization. *AIChE Journal*, 62(7):2259-2270. https://doi.org/10.1002/aic.15219

Liu W, Li S, Baule A, et al., 2015. Adhesive loose packings of small dry particles. *Soft Matter*, 11(32):6492-6498. https://doi.org/10.1039/C5SM01169H

Liu ZG, Wang PK, 1997. Pressure drop and interception efficiency of multifiber filters. *Aerosol Science and Technology*, 26(4):313-325. https://doi.org/10.1080/02786829708965433

Luding S, 2008. Cohesive, frictional powders: contact models for tension. *Granular Matter*, 10(4):235-246. https://doi.org/10.1007/s10035-008-0099-x

Marshall JS, 2009. Discrete-element modeling of particulate aerosol flows. *Journal of Computational Physics*, 228(5):1541-1561. https://doi.org/10.1016/j.jcp.2008.10.035

Marshall JS, Li S, 2014. Adhesive Particle Flow. Cambridge University Press, New York, USA, p.86-99.

Maze B, Vahedi Tafreshi H, Wang Q, et al., 2007. A simulation of unsteady-state filtration via nanofiber media at reduced operating pressures. *Journal of Aerosol Science*, 38(5):550-571. https://doi.org/10.1016/j.jaerosci.2007.03.008

Myojo T, Kanaoka C, Emi H, 1984. Experimental observation of collection efficiency of a dust-loaded fiber. *Journal of Aerosol Science*, 15(4):483-489. https://doi.org/10.1016/0021-8502(84)90044-2

Novick VJ, Higgins PJ, Dierkschiede B, et al., 1990. Efficiency and mass loading characteristics of a typical HEPA filter media material. Proceedings of the 21st DOE/NRC Nuclear Air Cleaning Conference, 2:782-798.

Roussel N, Nguyen TLH, Coussot P, 2007. General probabilistic approach to the filtration process. *Physical Review Letters*, 98(11):114502. https://doi.org/10.1103/PhysRevLett.98.114502

Schiller S, Schmid H, 2015. Highly efficient filtration of ultrafine dust in baghouse filters using precoat materials. *Powder Technology*, 279:96-105.

Tamadondar MR, Rasmuson A, Thalberg K, et al., 2017. Numerical modeling of adhesive particle mixing. *AIChE Journal*, 63(7):2599-2609. https://doi.org/10.1002/aic.15654

Thomas D, Contal P, Renaudin V, et al., 1999. Modelling pressure drop in HEPA filters during dynamic filtration. *Journal of Aerosol Science*, 30(2):235-246. https://doi.org/10.1016/S0021-8502(98)00036-6

Thomas D, Penicot P, Contal P, et al., 2001. Clogging of fibrous filters by solid aerosol particles: experimental and modelling study. *Chemical Engineering Science*, 56(11):3549-3561. https://doi.org/10.1016/S0009-2509(01)00041-0

Tien C, Teoh SK, Tan RBH, 2001. Cake filtration analysis—the effect of the relationship between the pore liquid pressure and the cake compressive stress. *Chemical Engineering Science*, 56(18):5361-5369. https://doi.org/10.1016/S0009-2509(01)00263-9

Tomas J, 2007. Adhesion of ultrafine particles—a micromechanical approach. *Chemical Engineering Science*, 62(7):1997-2010. https://doi.org/10.1016/j.ces.2006.12.055

Wang H, Zhao H, Guo Z, et al., 2013. Lattice Boltzmann method for simulations of gas-particle flows over a backward-facing step. *Journal of Computational Physics*, 239:57-71. https://doi.org/10.1016/j.jcp.2012.12.032

Wang J, Pui DYH, 2009. Filtration of aerosol particles by elliptical fibers: a numerical study. *Journal of Nanoparticle Research*, 11(1):185-196. https://doi.org/10.1007/s11051-008-9422-z

Yang M, Li S, Yao Q, 2013. Mechanistic studies of initial deposition of fine adhesive particles on a fiber using discrete-element methods. *Powder Technology*, 248:44-53. https://doi.org/10.1016/j.powtec.2012.12.016

Zhu HP, Zhou ZY, Yang RY, et al., 2008. Discrete particle simulation of particulate systems: a review of major applications and findings. *Chemical Engineering Science*, 63(23):5728-5770. https://doi.org/10.1016/j.ces.2008.08.006

中文概要

题　目：离散元-计算流体动力学耦合方法模拟多纤维阵列过滤微米级颗粒

目　的：微米细颗粒在不同纤维排列所组成的滤料中的沉积和穿透行为仍然缺少研究。本文通过离散元-计算流体动力学耦合（DEM-CFD）双向耦合方法，研究前加密、后加密以及规则错列阵列纤维在过滤压降和捕捉效率方面的特性。

创新点：1. 使用 DEM-CFD 流固双向耦合方法，建立了适用于多纤维阵列过滤微米颗粒的数值模拟方法；2. 得到并对比了不同排列形式的过滤压降和捕捉效率。

方　法：1. 通过数值模拟，得到顺列和错列排布纤维的过滤压降及捕捉效率（图 2 和 3、表 2）；2. 通过数值模拟，分析前加密、后加密错列排布纤维与规则错列排列纤维的优劣（图 6 和 7），并得出颗粒在滤料中的沉积分布（图 8）。

结　论：1. 错列纤维比顺列纤维提前进入堵塞期，在沉积相同颗粒数时具有更低的压降，且在清洁滤料期具有更高的捕捉效率；2. 前加密错列排布比后加密错列排布更早进入堵塞期，且总体穿透颗粒数量更少；3. 前加密错列排布适用于工业滤料，而后加密错列排布适用于一次性个人防护用品。

关键词：滤料过滤；纤维阵列；错列；离散元方法